

# CHARACTERIZATION OF THE INTERFACE BETWEEN STRAIN HARDENING CEMENTITIOUS REPAIR LAYERS AND CONCRETE SUBGRADE

CHRISTIAN WAGNER, NICK BRETSCHNEIDER AND VOLKER SLOWIK

Leipzig University of Applied Sciences (HTWK Leipzig)  
PF 301166, 04251 Leipzig, Germany  
e-mail: christian.wagner@fb.htwk-leipzig.de, www.htwk-leipzig.de

**Key words:** Interface, Strain hardening, Fiber reinforced concrete, Patch repair, Inverse analysis

**Abstract:** Results of experimental investigations into the mechanical behavior of the interface between strain hardening cement-based composites (SHCC) and concrete are presented. Wedge splitting tests served for the determination of the mode I fracture properties of the interface. The corresponding stress-crack opening curves were determined by inverse analysis of the experiments. Expectedly, they strongly depend on the roughness of the concrete surface if this roughness is smaller than a certain threshold value. Tests of the interface under combined tension and shear loading were also performed. The identification of the material parameters controlling the interface behavior under this type of loading will also require inverse analyses of the experiments.

## 1 INTRODUCTION

Strain hardening cement-based composites (SHCC) have proved to be suitable materials for repair layers on cracked concrete surfaces. For the durability of such covering layers, not only the mechanical behavior of the SHCC, but also the interface properties are of importance. Inadequate bond behavior may lead to local damages like chipping or, eventually, to the failure of the whole repair layer.

The behavior of interfaces between cementitious materials depends on a variety of influences, as are the surface roughness and cleanness, the properties of the fresh material, the casting and curing methods as well as the mechanical properties of the hardened materials. During the last decades, the behavior of such interfaces was investigated in numerous experimental studies and appropriate material models have been developed. In most cases, interfaces between quasi-brittle cementitious materials were subject of the investigations. Recently developed strain

hardening materials may require adjusted or extended mechanical models for the interface behavior which account for the high deformability of these materials. The intention of the authors was to investigate the bond between SHCC repair layers and concrete subgrade in order to appropriately model and optimize the behavior of such layers.

For the experimental investigation of bond properties, different types of experiments and setups were proposed. An overview has been published by Silfwerbrand et al. [1]. These authors consider a comparison of bond properties obtained in different types of tests as problematic. This may be attributed to significant influences of specimen geometry and size on the stresses and displacements in the interface. Another problem are the technical difficulties to impose pure shear on an interface. Interface tests under combined normal and shear loading are easier to perform, but still challenging from the technical point of view.

The so-called slant shear test is often used for the characterization of repair materials. In

this test, an interface is subjected to a combined compressive and shear loading. A prismatic specimen with an inclined joint is loaded in the uniaxial direction. Austin et al. [2] discussed the advantages and drawbacks of the slant shear test. The realistic loading conditions of the interface are considered to be an advantage. On the other hand, the moduli of elasticity of the two adjacent materials have a strong influence on the stress concentrations at the edges of the interface. It has also to be considered that bond failure will only occur when the surface roughness and, consequently, the interface shear strength are low. Otherwise, the specimen will exhibit a compressive failure with the formation of characteristic longitudinal splitting cracks. This failure mode is likely to occur especially in the case of flat joint inclinations. The slant shear test with compressive loading is reasonable only for steeper inclinations, preferably above  $60^\circ$ . In addition, the ratio of the bond strength to the material's strength should be smaller than one.

Damage patterns observed at real cement-based covering layers show that the interfaces to the subgrade are failing predominantly under tension or under combined tension-shear loading. For this reason, the bond behavior under these types of loading was subject of the present investigation.

For the tensile loading (mode I) wedge splitting tests were conducted and for the combined tension-shear loading (mode I & mode II, i.e., mixed mode) the setup of the slant shear test has been adopted, see Section 2.4. The last-mentioned test allows to vary the tension-shear ratio by changing the inclination of the joint. It is impossible, however, to directly separate the damage levels reached under tension and shear, respectively. Therefore, inverse analyses of the experiments are required. In these analyses, the non-uniform stress distribution along the interface is also accounted for. An appropriate material model describing the softening under tension and shear may be identified in this way. The present paper contains the inverse analysis results for the wedge splitting tests (mode I). For the case of combined loading (mixed mode), the inverse analyses are still

being carried out. The corresponding tension-shear test results, however, will be presented here.

## 2 EXPERIMENTAL PROGRAM

As stated before, two different test setups were used for the experimental investigations. The specimens for the wedge splitting tests (mode I) consisted of two materials with an interface along the ligament, i.e., along the expected crack path, see Figure 1. One half of the respective specimen was made of SHCC, the other one of high-strength concrete. The surface roughness in the interface was varied and, for a comparison, reference specimens without interface and consisting only of SHCC were tested.

For the tension-shear tests (mixed mode), the setup has been derived from the slant shear test, see Figure 2. The latter has originally been proposed for compression-shear loading and in the literature several critical discussions on the validity of the test results may be found. For the tests performed here, the original setup was modified and the final interpretation of the results will be based on inverse analyses of the tests.

A total of about 45 wedge splitting tests and 30 slant tension-shear tests were conducted.

### 2.1 Materials

For the concrete subgrade, a high-strength concrete, see Table 1, was used. Hence, failure of the concrete subgrade was unlikely to occur.

**Table 1:** Material composition for the concrete subgrade.

Material	Content by mass [kg/m <sup>3</sup> ]	Content by mass [kg]
Cement CEM I 42.5 R	420	1.00
Fly ash	80	0.19
Silica fume	30	0.07
Water	168	0.40
Aggregates (0/8 mm)	1699	4.05
Superplasticizer	10.5	0.025

Table 2 contains the material composition for the repair material (SHCC). Polyvinyl alcohol (PVA) fibers from Kuraray, Japan, with a length of 8 mm and a diameter of 0.04 mm were used as reinforcement. The fiber content amounted to 2.0 % by volume. The material design was aimed at a high strain capacity.

**Table 2:** Material composition for the SHCC repair material.

Material	Content by mass [kg]
Cement CEM I 42.5 R	1.00
Fly ash	1.18
Water	0.68
Quartz sand (0/0.25 mm)	0.98
Superplasticizer	0.027
Stabilizer	0.015
PVA fibers	2.00 % by volume

**Table 3:** Material properties.

Material	Compressive strength [MPa]	Elastic modulus [GPa]
Concrete (28 days)	86.3	37.4
SHCC (28 days)	47.5	18.4

The application of the SHCC to the concrete subgrade took place when the latter had reached an age of 14 days. The actual interface tests were conducted 28 days after the application of the SHCC, i.e., 42 days after casting the high-strength concrete samples. The mechanical properties of both materials are listed in Table 3.

## 2.2 Specimen preparation and surface characterization

For preparing the specimens for the wedge splitting tests (WS), concrete beams with a cross-section of 150 x 155 mm<sup>2</sup> and a length of 500 mm were cast. After one week, they have been split longitudinally and the cast surfaces (150 x 500 mm<sup>2</sup>) of the two halves (WS1-WS8) were sandblasted until the aggregate particles were exposed. For quantifying the surface roughness, sand patch tests were carried out. The measured depths of roughness are listed in Table 4.

**Table 4:** Surface roughness of the sandblasted concrete beams.

Wedge splitting tests	Depth of roughness [mm]	Slant tension-shear tests	Depth of roughness [mm]
WS1	0.41	SS00	0.27
WS2	0.35	SS20	0.26
WS3	0.47	SS40	0.29
WS4	0.36	SS60a	0.34
WS5	0.38	SS75a	0.32
WS6	0.43	SS90a	0.33
WS7	0.35	SS60b	0.41
WS8	0.29	SS75b	0.39
		SS90b	0.37

The SHCC repair material was applied to the sandblasted surfaces with a layer thickness of 75 mm. Prior to the wedge splitting tests, slices with a thickness of 100 mm have been cut out of the beams and served as test specimens. The notches were saw cut.

The specimens for the slant tension-shear tests (SS) were prepared in a similar way. However, in order to obtain inclined interfaces, the concrete beams (SS00-SS90) were cast into oblique-angled forms. Surface preparation and characterization have been conducted as in the case of the specimens for the wedge splitting tests. Slices with a thickness of 70 mm were cut out of the beams and notched as explained in Section 2.4.

## 2.3 Setup for the wedge splitting tests

For the wedge splitting tests, specimens with a length of 150 mm, a height of 150 mm and a thickness of 100 mm were used. The experimental setup is shown in Figure 1. The notch length has been varied. Table 5 contains the specimen dimensions.

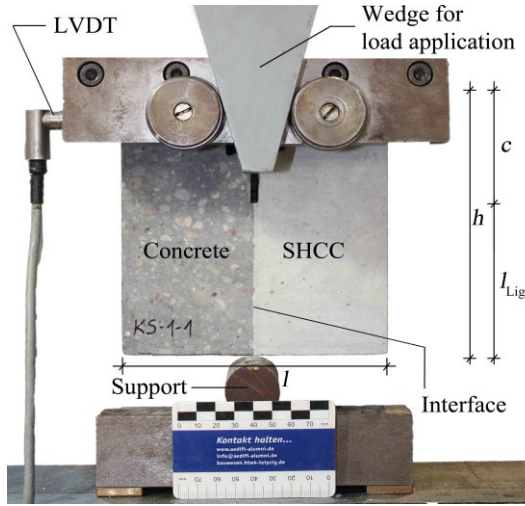


**Figure 1:** Experimental setup for the wedge splitting tests.

**Table 5:** Specimen dimensions for the wedge splitting tests.

	Length $l$ [mm]	Height $h$ [mm]	Thickness $t$ [mm]	Ligament length $l_{Lig}$ [mm]
I	150	150	100	90
II	150	150	100	75
III	150	100	100	60

Two LVDTs with a base length of 40 mm have been used for measuring the CMOD between the load application points. The tests were performed in a comparatively stiff 100 kN loading frame under displacement control with 0.2  $\mu\text{m/s}$ .

## 2.4 Setup for the slant tension-shear tests

In contrast to the specimen geometry originally proposed for the slant shear tests, two notches were cut into the specimens used here, see Figure 2. The remaining interface area was 70 x 70 mm<sup>2</sup> for all inclinations  $\alpha$  of the interface. There are two reasons for these notches. On one hand, the influence of the near-surface material properties was to be excluded. In the vicinity to the formwork, the local properties may be different from those in the bulk, for instance due to the aggregate particles arrangement. On the other hand, without the notches acute-angled edges will be formed in both halves of the specimen, i.e., in the concrete as well as in the SHCC. In these regions, failure of the material itself may occur

instead of bond failure. This would distort the results of the interface test.

By varying the joint inclination  $\alpha$ , the state of stress in the interface is changed. In the experiments performed here, specimens with six different angles (0°, 20°, 40°, 60°, 75°, and 90°) were tested. An angle of zero results in pure tension and an angle of 90° theoretically in pure shear. Figure 2 shows a specimen with a joint inclination of 60°.

During the tests, two orthogonal displacement components between two points at each notch tip were measured by using LVDTs, see Figure 2. On the basis of these measured displacement values, the normal and tangential displacements in the interface could be calculated, i.e.,  $\Delta u$  and  $\Delta v$  in Figure 2.

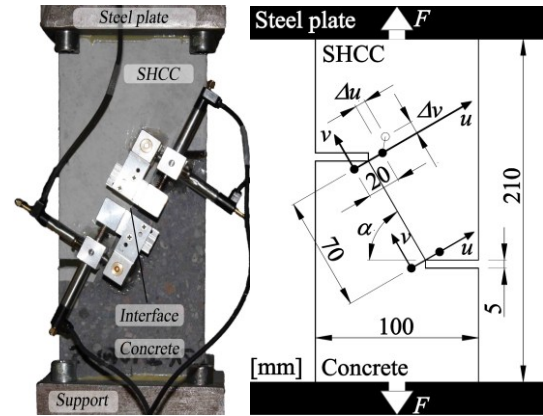


**Figure 2:** Experimental setup for the slant tension-shear tests.

Two additional LVDTs were attached to the backside of each specimen. They served for measuring the vertical notch tip opening displacement which was used as feedback signal for the closed-loop controlled test. The loading velocity amounted to 0.1  $\mu\text{m/s}$ .

## 3 EXPERIMENTAL RESULTS

### 3.1 Results of the wedge splitting tests

The results of the wedge splitting tests are presented in Figures 3-5 for the different ligament lengths. It may be seen that the curves show a comparatively large scatter. This may be explained by the locally different failure behavior. In a certain portion of the fracture surface, the SHCC remains attached to

the interface, i.e., the final crack is formed in the SHCC rather than in the interface. The interface portion with SHCC adherence strongly influences the bond properties. This will be discussed in Section 4.

Some of the wedge splitting tests with the longest ligament length, see Figure 3, became unstable after reaching the peak load and were excluded from the following evaluation.

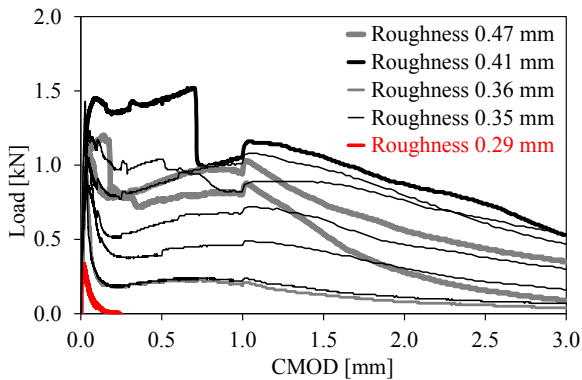


**Figure 3:** Load-displacement curves for the wedge splitting tests with a ligament length of 90 mm.

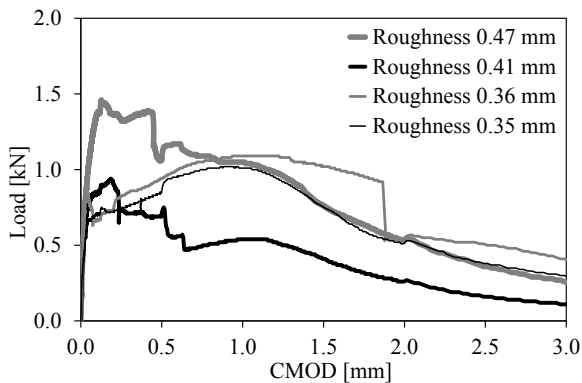


**Figure 4:** Load-displacement curves for the wedge splitting tests with a ligament length of 75 mm.

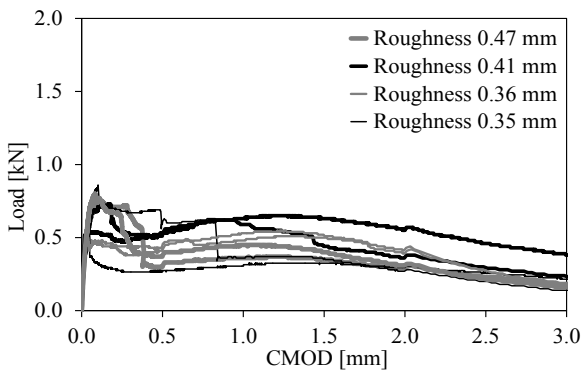


**Figure 5:** Load-displacement curves for the wedge splitting tests with a ligament length of 60 mm.

It has to be considered that the roughness values given in Figures 3-5 are average values for the respective concrete beam the individual specimens were originating from, see Section 2.2. Exact roughness values for the individual specimens are not known. An evaluation of the obtained fracture surfaces is under way.

The results of the wedge splitting tests of SHCC specimens without interface are presented in Figure 6. The maximum loads are significantly higher than in the tests with interfaces. In order to enforce a localized fracture, grooves along the crack path were cut into the front and back faces of the specimens. In this way, the ligament has been weakened and the width of the fracture process zone was confined. The intention was to allow for a comparison with the bond failure observed in the specimens with interface.

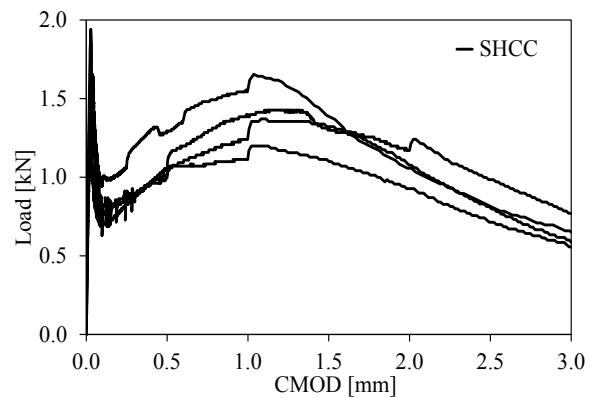


**Figure 6:** Load-displacement curves for the wedge splitting tests of SHCC specimens.

### 3.2 Results of the slant tension-shear tests

For each test, five load-displacement curves were obtained, two for the tangential displacement, two for the normal displacement, and one for the longitudinal displacement measured at the backside of the specimen. Figure 7 shows individual curves obtained for the interface inclination of  $40^\circ$ . For the other inclinations, averaged curves are presented in Figure 8 as an overview.

The curves in Figure 7 belong to three different tests. They were measured at the upper notch tip and show a good agreement.

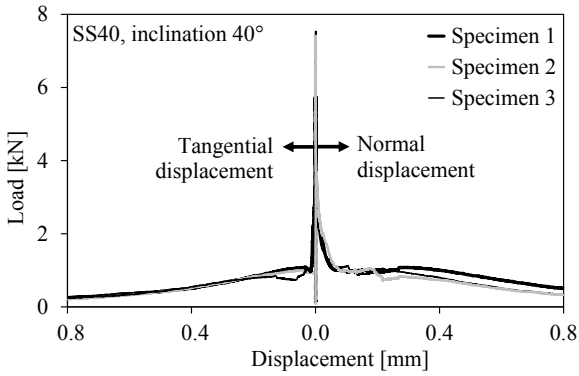


**Figure 7:** Load-displacement curves for the normal and tangential displacement in the interface at the upper notch tip.

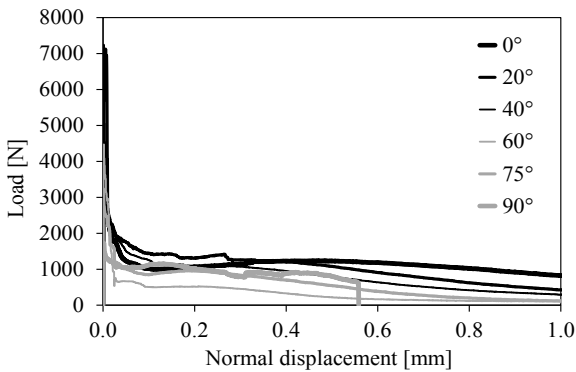


**Figure 8:** Load-displacement curves for the normal displacement at the upper notch tip.

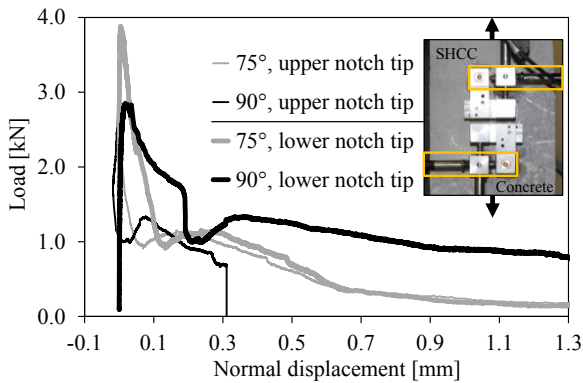


**Figure 9:** Comparison of the load-displacement curves for the normal displacement at the upper and lower notch tip.

When comparing the measured displacements at the upper and lower notch tip, differences may be found which are getting larger with increasing interface inclination, see Figure 9. This results from the non-uniform stress distribution in the interface and points to the necessity of inverse analyses of the experiments. These analyses will be performed

for determining the strength and softening properties of the interface under tension and shear.

## 4 DETERMINATION OF INTERFACE PROPERTIES BY INVERSE ANALYSIS

### 4.1 Interface properties for mode I

The determination of the uniaxial stress-crack opening curves for the interface requires the inverse analysis of the conducted wedge splitting tests. This analysis includes simulations of the fracture process and the iterative fitting of the numerical results to the experimental ones. Objective inverse analysis results require very good fits, i.e., comparatively small error values. For this reason, the applied optimization procedure is based on an evolutionary algorithm [4].

The stress-crack opening curves obtained by inverse analysis are presented in Figures 10-12. As expected, these curves have a similarly large scatter like the measured load-displacement curves shown in Figures 3-5. As stated before, this is attributed to the significant influences of the surfaces roughness and of the different interface portions with adhering SHCC. The SHCC adherence is also considered to be the reason for the hardening effect which is observed in many stress-crack opening curves after the steep post-peak stress drop.

It has to be taken into account that the inverse analysis of the wedge splitting tests is based on the assumption of uniform fracture properties within the ligament. Since the final crack will be formed partially along the interface and partially in the SHCC, this assumption is no longer fulfilled for the particular type of failure investigated here. The measured load-displacement curve will not only be influenced by the total area portion with SHCC adherence, but also by the location of such areas within the ligament. This also contributes into the observed comparatively large scatter of the stress-crack opening curves, see Figures 10-12.

When comparing the inverse analysis results obtained for the different specimen geometries, no systematic influence of the ligament length may be identified. It has to be considered, however, that for the longest ligament length not all the samples were included in the evaluation since unstable fracture occurred in some tests, see Section 3.1.

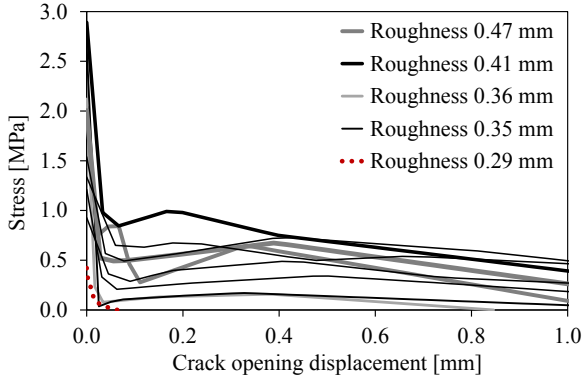


**Figure 10:** Softening curves obtained by inverse analysis of the wedge splitting tests with a ligament length of 90 mm.

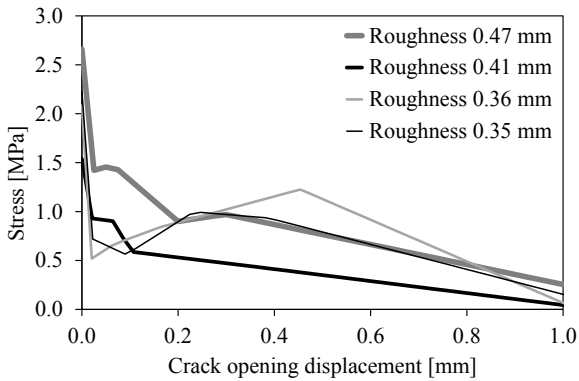


**Figure 11:** Softening curves obtained by inverse analysis of the wedge splitting tests with a ligament length of 75 mm.

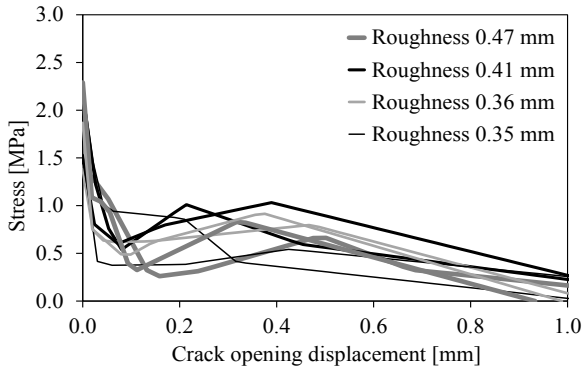


**Figure 12:** Softening curves obtained by inverse analysis of the wedge splitting tests with a ligament length of 60 mm.

Table 6 contains the obtained values for the uniaxial tensile strength and for the fracture energy. For series WS1, WS2, WS3, WS4, and WS7 no clear correlation between bond tensile strength and surface roughness (0.35-0.47 mm) may be seen. For Series WS8, however, which is characterized by a low surface roughness (0.29 mm), significantly lower values for the tensile strength were measured.

**Table 6:** Results of the inverse analysis of the wedge splitting tests.

Wedge splitting (WS) tests	Depth of roughness [mm]	Tensile strength [MPa]	Fracture energy [N/m]
WS1-I-2	0.41	2.89	839
WS1-II	0.41	1.54	375
WS1-III-1	0.41	2.17	636
WS1-III-2	0.41	1.52	751
WS2-I-2	0.35	2.64	137
WS2-II	0.35	2.23	661
WS2-III-1	0.35	2.23	424
WS2-III-2	0.35	1.54	482
WS3-I-1	0.47	2.04	431
WS3-I-2	0.47	2.00	565
WS3-II	0.47	2.66	800
WS3-III-1	0.47	2.57	412
WS3-III-2	0.47	2.29	478
WS4-I-1	0.36	2.12	97
WS4-II	0.36	2.08	773
WS4-III-1	0.36	1.38	563
WS4-III-2	0.36	1.87	546
WS5-I-1	0.38	1.63	11
WS5-I-2	0.38	1.28	7
WS5-I-3	0.38	1.29	7
WS5-I-4	0.38	1.29	7
WS6-I-1	0.43	0.85	23
WS6-I-2	0.43	0.89	22
WS6-I-3	0.43	1.52	25
WS6-I-4	0.43	1.01	26
WS7-I-1	0.35	1.21	339
WS7-I-2	0.35	1.54	851
WS7-I-3	0.35	1.34	1032
WS7-I-4	0.35	0.93	555
WS8-I-1	0.29	0.48	5
WS8-I-2	0.29	0.37	6
WS8-I-3	0.29	0.42	6
WS8-I-4	0.29	0.30	5

A higher surface roughness results in a more pronounced post-peak hardening and, consequently, in a higher fracture energy. This is due to the larger interface portion with adhering SHCC in the case of the higher roughness.

It was observed that for low roughness values of the interface, the high deformability of the SHCC has nearly no effect on the bond behavior. This shows the comparison of the curves for SHCC and unreinforced repair mortar (matrix of the SHCC without fibers) with the lower roughness value in Figure 13. The specimens with PVA fibers (SHCC) and without fibers exhibit nearly the same post-peak behavior. The low surface roughness prevents SHCC adherence and the fiber reinforcement can not be activated.

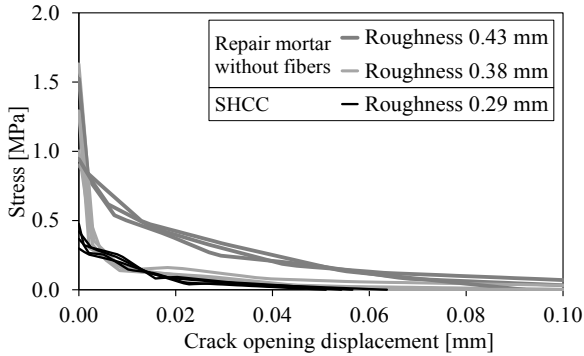


**Figure 13:** Stress-crack opening curves obtained by inverse analysis of wedge splitting tests.

In Figure 13 it may also be seen that the interface with the unreinforced material and the higher surface roughness exhibits a much more ductile fracture behavior.

Silfwerbrand [3] stated that there is a certain threshold value for the surface roughness of interfaces. If this threshold value is exceeded, a further increase of the roughness will no longer influence the bond strength. According to Silfwerbrand et al. [1], this threshold roughness is in the order of magnitude of the one of typical sandblasted concrete surfaces.

On the basis of the results presented here, it is speculated that above the aforementioned roughness threshold value the high deformability of the SHCC is activated resulting in a ductile bond behavior. Below this threshold

value, the ductility of the bond depends on both the surface roughness and the deformability of the repair material. If the surface roughness is getting even lower, the influence of the material's deformability vanishes and, eventually, the fiber reinforcement will no longer have an effect. This was probably the case for the SHCC results presented in Figure 13. When the curves for SHCC in Figure 13 are compared to those in Figures 10-12, however, a strong effect of the material's deformability on the bond behavior may be seen. Because of the higher surface roughness, SHCC is adhering to the interface resulting in a significantly larger critical crack opening displacement (average value about 1.20 mm), see Figures 10-12, and in a significantly higher fracture energy. In addition, many curves in Figures 10-12 show a characteristic second peak in the post-peak range which is also attributed to the SHCC adherence. If a ductile bond behavior is to be achieved, the high deformability of SHCC can only be utilized when the surface roughness is sufficiently high. The bond strength has to exceed the strength of the SHCC.

After the wedge splitting tests, the interface area portions with SHCC adherence were determined. Figure 14 shows the relationship between this area portion and the fracture energy. An almost linear dependency is observed. For 100 % adherence, the fracture energy values determined in the wedge splitting tests of the SHCC specimens without interface, see Section 3.1, were used. In these tests, the highest fracture energy values have been measured. It should be noted, however, that in case of uniaxial tension and perfect bond, the formation of multiple parallel cracks may result in significantly higher fracture energy values. In the wedge splitting tests performed here, this multiple cracking was constricted.

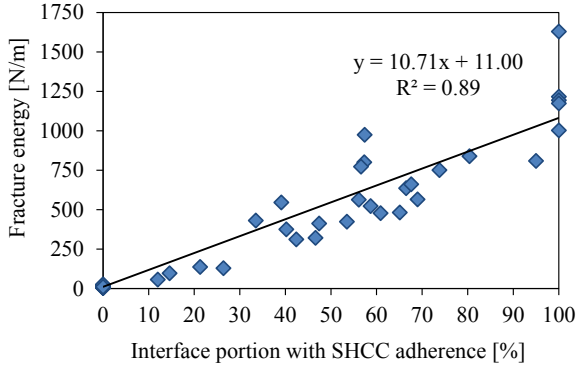


**Figure 14:** Relationship between the fracture energy and the interface portion with SHCC adherence.

## 4.2 Interface properties for mixed mode

The inverse analyses of the slant tension-shear tests are still under way. Nevertheless, some characteristic experimental results are presented in the following.

The ultimate stresses for different interface inclinations are shown in Figure 15 by means of a Mohr-Coulomb type presentation. The dots (labeled as Slant tension-shear tests) correspond to the normal and shear stresses obtained under the assumption of a uniform stress distribution in the interface. An improved stress analysis yielded the circles (labeled as Slant tension-shear tests adjusted). Thereby, the stress distributions have been determined by linear-elastic finite element analyses.

Figure 15 also shows a failure function (solid line) which is expressed according to Červenka et al. [5] by Eq. 1.

$$F = (\tau_1^2 + \tau_2^2) - a - b = 0 \quad (1)$$

with

$$a = 2 \cdot c \cdot \tan(\phi_f) \cdot (\sigma_t - \sigma)$$

$$b = \tan^2(\phi_f) \cdot (\sigma^2 - \sigma_t^2)$$

where  $\tau_1$  and  $\tau_2$  = shear stresses,  $\sigma_t$  = tensile strength,  $\sigma$  = normal stress,  $\phi_f$  = angle of friction, and  $c$  = cohesion. The material properties adopted here for this failure function are listed in Figure 15.

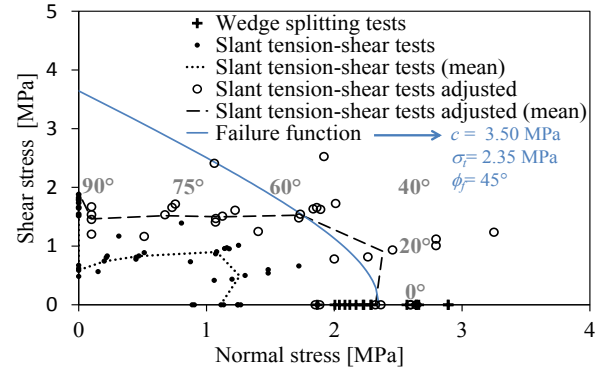


**Figure 15:** Ultimate stresses in the slant tension-shear tests.

It is assumed that the bond strength is underestimated by the simplified evaluation of the test results. As repeatedly stated before, inverse analyses of the experiments are required.

## 5 CONCLUSIONS

For characterizing the mode I fracture behavior of an interface between SHCC and concrete subgrade, wedge splitting tests and inverse analyses of these tests were carried out. The following conclusions may be drawn:

- If the surface roughness of the interface is low, the bond strength depends strongly on the roughness values.
- If the bond strength is high, cracks will be formed in the SHCC and the fibers are activated. In this case, the influence of the surface roughness on the bond strength vanishes.
- The higher the area portion with an intact bond between SHCC and concrete, i.e., the higher the area portion with SHCC adherence, the more ductile the bond behavior will be.
- The mode I fracture energy strongly depends on the portion of the fracture surface with SHCC adherence.
- If the bond strength is low when compared to the matrix strength, the interface will fail and the SHCC properties do not have an influence on the bond behavior.

For investigating the interface behavior under combined tension and shear (mixed mode) loading the slant shear test has been adopted. Although the inverse analyses of these tests are still to be completed, the following preliminary conclusions may be drawn:

- The proposed experimental setup for a modified slant shear test has proved to be applicable. Reproducible test results were obtained which may serve as a basis for the inverse analyses.
- A first simplified evaluation of the test results yielded a failure surface with the expected shape. It has also shown a strong non-uniformity of the stress distribution within the ligament. An exact evaluation of the experimental results requires inverse analyses of the tests.

#### ACKNOWLEDGEMENT

The first author would like to acknowledge the financial support by the European Social Fund (ESF).

#### REFERENCES

- [1] Silfwerbrand, J., Beushausen, H. and Courard, L., 2011. Bond. In Bissonnette et al. (eds.), *Bonded Cement-Based Material Overlays for the Repair, the Lining or the Strengthening of Slabs or Pavements, State-of-the-Art Report of the RILEM Technical Committee 193-RLS*; pp.51-79.
- [2] Austin, S., Robins, P. and Pan, Y., 1999. Shear bond testing of concrete repairs. *Cement and Concrete Research* **29**(7):1067-76.
- [3] Silfwerbrand, J., 1990. Improving concrete bond in repaired bridge decks. *Concrete International* **12**(9):61-66.
- [4] Slowik, V., Villmann, B., Bretschneider, N., 2006. Computational aspects of inverse analyses for determining softening curves of concrete. *Computer Methods in Applied Mechanics and Engineering* **195**(52):7223-36.
- [5] Červenka, J., Kishen, C. and Saouma, V.E., 1998. Mixed mode fracture of cementitious bimaterial interfaces; Part II: Numerical simulation. *Engineering Fracture Mechanics* **60**(1):95-107.